# Simulation of a hybrid vehicle powertrain having direct methanol fuel cell system through a semi-theoretical approach

[1,2*]Mustafa Umut Karaoğlan, [2,3]Alper Can İnce, [1]C. Ozgur Colpan, [4]Andreas Glüsen, [1]Nusret Sefa Kuralay, [4]Martin Müller, [4]Detlef Stolten

[1] Dokuz Eylul University, Faculty of Engineering, Mechanical Engineering Department, Tinaztepe, Buca, Izmir, 35397, Turkey
[2] Dokuz Eylul University, The Graduate School of Natural and Applied Sciences, Mechanical Engineering Department, Tinaztepe, Buca, Izmir, 35397, Turkey
[3] Gebze Technical University, Faculty of Engineering, Mechanical Engineering Department, Gebze, Kocaeli, 41400, Turkey
[4] Forschungszentrum Jülich GmbH, Institute of Energy and Climate Research - Electrochemical Process Engineering (IEK-3), 52425, Jülich, Germany

* E-mail: mustafa.karaoglan@deu.edu.tr

**Abstract**
Different operating scenarios can be used in a hybrid system based on a direct methanol fuel cell (DMFC) and a battery. In this paper, a DMFC system model is integrated into a model formed for a hybrid vehicular system which consists of a battery, a DMFC stack and its auxiliary equipments; and the model is simulated in Matlab/Simulink environment using a quasistatic approach. An algorithm for the energy management of the system is also developed considering the state of charge (SOC) of the battery. In the DMFC system model, the current and empirical data for the polarization curves as well as methanol crossover and water crossover rates are taken as the input parameters, whereas the stack voltage, the remaining methanol in the fuel tank, and the power demand of auxiliary equipments are taken as the output parameters. In this model, the methanol consumption, and the water and $CO_2$ production are found applying mass balances for each component of the system. The results of the simulations help to give more insights into the operation of a DMFC based hybrid system.

**Keywords:** DMFC, fuel cell system, quasistatic model, vehicular application

## 1. Introduction

Due to the increasing concerns on environmental problems (e.g. climate change and air pollution) and diminishing petroleum reserves, fuel cells, which generally offer better environmental impact and higher electrical efficiency, have become popular for vehicular applications in the recent years. Among the different fuel cell types, direct methanol fuel cells (DMFC) should be preferred especially for small vehicles. Its main advantage stems from the fact that it uses liquid diluted methanol solution, which is easy to store and obtain. However, undesired methanol crossover from anode to cathode, low electrochemical reaction rates at both anode and cathode, and thermal management (especially for large stacks) are the main challenges towards their widespread use in these applications. In addition, water crossover from anode to cathode has an adverse effect on water management owing to cathode flooding and excessive anodic water consumption [1]. In general, methanol ($CH_3OH$) mixed with recycled water (generated at the cathode compartment) is used as fuel in DMFC systems, while carbon dioxide ($CO_2$) occurs as product. In these systems, operating conditions (e.g. temperature, methanol concentration, and flow rate of the reactants) play a significant role for their performance. A DMFC can be designed as a passive or an active system. In a passive system, air is fed to system by natural flow, i.e. self breathing. This system is small and more convenient for low power applications (e.g. portable charger for mobile phones) but it has less ability to control over the operating parameters such as fuel and air stoichiometry. On the other hand, an active system, which includes balance of plant components such as pump and blower, can be used for higher power applications (e.g. auxiliary power unit for recreational activities). In this system, fuel and air flow rates can be controlled; and it is generally more energy-efficient [2].

Fuel cell (FC) research, demonstration and commercialization in the automotive industry have been proceeding increasingly due to the growing need for clean and efficient driving with long range. Significant progress has been achieved especially on the research for the development of DMFC based vehicles. For example, Huang et al. [3] investigated a powertrain system composed of a battery and a DMFC unit to produce current for the electric motor in a DMFC hybrid electric vehicle application. Samsun et al. [4] performed an analysis of direct and indirect hybrid configurations for a truck with various operating strategies. Li et al. [5] and Marzougui et al. [6] investigated several energy management strategies (EMS) for a range-extended electric vehicle and a FC hybrid vehicle, respectively. EMS was also studied by Marx et al. [7] for FC hybrid vehicle applications that use multistack construction under various driving conditions such as urban, rural and highway. Li et al. [8] implemented a theoretical investigation, which includes system model, energy flow and system simulation, for a FC supercapacitor hybrid construction vehicle. Li et al. [9] performed fuel cell system degradation analysis for a plug-in FC hybrid city bus. In addition of heavy vehicle applications, Huang et al. [3] conducted a numerical investigation for assessing the performance of fuel cell hybrid scooter under urban driving conditions using a Simulink model. Mokrani et al. [10] studied system simulations of FC electric vehicle in both Simulink environment and experimentally according to a proposed EMS that includes various operating modes. Hwang et al. [11] performed a system simulation for power management

system (PMS) of a FC hybrid vehicle in Simulink and subsystems of the model were detailed for the dynamic model of the FC hybrid vehicle. Zheng et al. [12] used a rule-based PMS to simulate FC hybrid vehicle to find fuel consumption by optimal control and they compared it with equivalent fuel consumption results.

Several studies on DMFC modeling at cell (e.g. [13,14,15,39]) and stack (e.g. [16-18]) levels can be found in the literature. However, there are limited DMFC modeling studies on the system-level. One of the earliest studies on the steady-state modeling and simulation of the DMFC systems was published by von Andrian and Meusinger [19], who examined the effects of the operating conditions such as temperature, pressure, air to fuel ratio, and methanol permeation on the fuel cell system performance (e.g. electrical efficiency of the system). They found that reducing the air to fuel ratio leads to a higher electrical efficiency. In addition, it was found that when the amount of permeating methanol increases, the system efficiency reduces dramatically. Dohle et al. [20] described the heat and power management of a DMFC system through modeling and experimental investigation of this system. They presented the modeling equations including mass, energy, and heat balances for this system. The results of their study showed that the system pressure and the air flow rate have an important impact on both the power output and electrical efficiency of the system. Furthermore, they found that the vaporization of water at the cathode influences the heat balance of the cell. Jiang and Chu [21] examined the recycled water percentage under cell operating conditions through a system-level model. For this purpose, water crossover data obtained from a DMFC stack model was used. Their results indicated that 98% of the water from the cathode outlet must be recycled at an average cell voltage of 0.33 V and a cell temperature 62 °C. An alternative approach for modeling a DMFC system was developed by Na et al. [22]. They focused on reducing the high amount of methanol loss due to evaporation in the separator and mixer. Therefore, they modified their previous system, which they called “Mingled Outlet System” as described in a prior publication ([23]) and called the new system as “Highly Integrated System”. In their study, they compared both systems in terms of concentration, temperature, water recovery controllability, and efficiency. The results of their study showed that “Highly Integrated System” offers better system efficiency and fewer components than “Mingled Outlet System” due to less methanol evaporation in the separator.

In this study, firstly, using the DMFC model developed in Matlab/Simulink environment, the amount of the methanol consumption, water production and consumption, $CO_2$ production, and required air are found. This model can be regarded as a semi-theoretical model as the cell voltage, water crossover rate, and methanol permeation rate with respect to current density were obtained experimentally for various methanol concentrations. Then, a system-level model of the DMFC and battery-based powertrain system of a vehicle was developed using the same software. This system consists of a battery as the primary energy source and a DMFC stack for the charging the battery. The configuration of this system is similar to the range-extended FC hybrid vehicle given in the paper by Fernandez et al. [24]. Unlike the DMFC system-level modeling papers found in the literature, the modeling and simulation of the FC hybrid vehicle is based on a semi-theoretical approach in which experimental DMFC data and a theoretical powertrain model are combined.

## 2. System-Level Modeling

In this study, a small-sized fuel cell hybrid vehicle system consisting of an electric motor, a battery, and a fuel cell for the power arragenments and DC/DC converters for the voltage arragenments was considered as a case study. In this system, battery is the main energy supplier of the electric motor; and the DMFC system is used to recharge the battery. Power requirement of the vehicle is provided by a DC electric motor when the vehicle is moving. The electric motor can also work as a generator that recovers braking energy and transmits it into the battery via a bidirectional DC/DC converter during the braking operation. A unidirectional DC/DC converter is located between the FC and the battery for boosting the voltage. The layout of the powertrain components adopted in this DMFC hybrid powertrain is illustrated in Fig. 1.

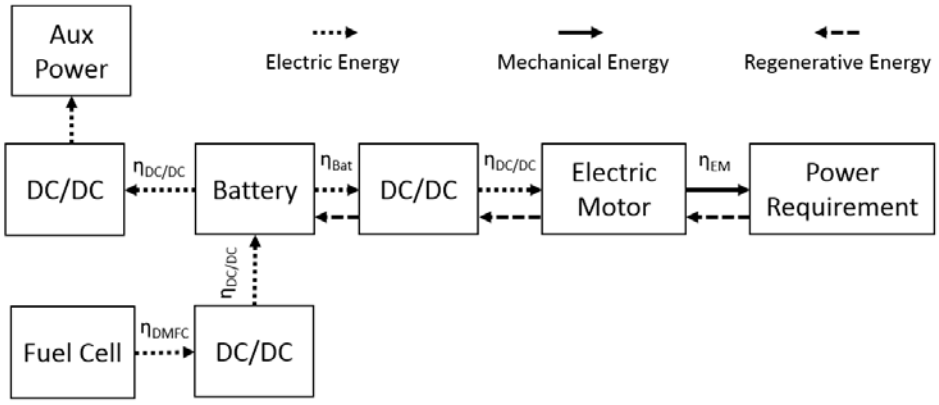


**Fig. 1** Structure of a fuel cell hybrid vehicle powertrain

### 2.1. Vehicle Model

The power required for the electric motor of a vehicular system can be calculated using the speed profile of the vehicle, which depends on the selected drive cycle as shown in Fig 2a. This cycle, which lasts 70 seconds, consists of three acceleration and two deceleration sections. The maximum vehicle speed is 15 km/h in this cycle. Power required for the electric motor during the drive cycle is determined using the longitudinal motion equations together with the parameters and drive cycle appropriate for a small-sized vehicle. In order to find the required power, the forces acting on the vehicle traction tires should be first calculated. These forces are the rolling resistance ($F_R$), air resistance ($F_L$), climbing resistance ($F_{ST}$), and acceleration resistance ($F_a$); and the equations required to find these forces are given below [8]. It should be noted that the following assumptions are made in this vehicle model: tire slip and system vibration are neglected; and dynamic tire radius is assumed to be constant.

$$F_R = m \cdot g \cdot f_R \tag{1}$$

$$F_{ST} = m \cdot g \cdot \sin\delta \tag{2}$$

$$F_L = \frac{1}{2} \cdot \rho \cdot A \cdot C_W \cdot V^2 \tag{3}$$

$$F_a = \lambda \cdot m \cdot a \tag{4}$$

Where m represents the total mass of the vehicle, $g$ is the gravity of acceleration (9.81 m/s$^2$), $f_R$ is the rolling resistant coefficient, $\delta$ is the slope angle of the road, $\rho$ is the density of air (1.2 kg/m$^3$), $C_W$ is the aerodynamic drag coefficient of the vehicle, A is the projection area of vehicle, $V$ is the velocity of vehicle, λ is the coefficient of the effect of rotating masses, and a is the acceleration of vehicle.

Required torque ($M_{EM}$) for the EM can be calculated using Eq. (5).

$$M_{EM} = \frac{\sum F \cdot \eta_M \cdot r_{dyn}}{i} \tag{5}$$

Where $r_{dyn}$ is the dynamic tire radius, $\eta_M$ is the mechanical efficiency of driveline, and i is the gear ratio between the motor and the tire which is assumed as fixed gear ratio. $\sum F$ represents the total resistance forces. The rotational speed of electric motor ($n_{EM}$) and the required power on the electric motor ($W_{EM}$) can be calculated using Eqs. (6) and (7) [8].

$$n_{EM} = \frac{V \cdot 60 \cdot i}{2\pi \cdot r_{dyn}} \tag{6}$$

$$W_{EM} = \frac{M_{EM} \cdot n_{EM}}{9549} \tag{7}$$

The input parameters for the vehicle model are given in Table 1. Using these parameters, the required power on EM as shown in Eq. 7, is calculated for the given speed profile of the vehicle. The results are shown in Fig. 2b. According to these results, maximum power of 350 W is needed on the EM when the vehicle reaches its the maximum speed.

**Table 1.** Input parameters of the vehicle model

| **Parameter** | **Value** |
|---|---|
| Vehicle mass (m) | 100 kg |
| Coefficient of rolling resistant ($f_R$) | 0.009 |
| Aerodynamic drag coefficient ($C_W$) | 0.28 |
| Projection area of vehicle (A) | 0.6 m$^2$ |
| Coefficient of the effect of rotating masses (λ) | 1.02 |
| Mechanical efficiency of driveline ($\eta_M$) | 0.9 |
| Dynamic tire radius ($r_{dyn}$) | 0.21 m |
| Gear ratio (i) | 2 |

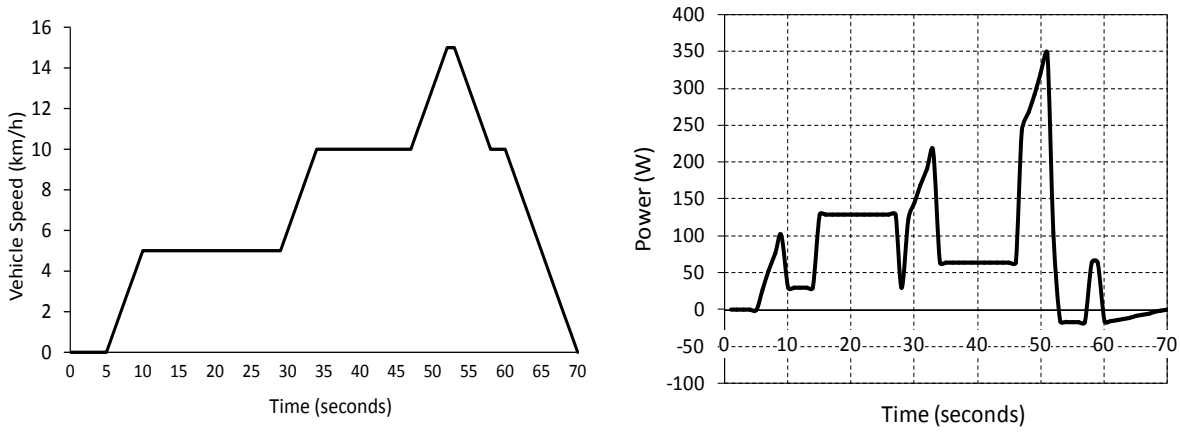


**Fig. 2** (a) Speed profile of the vehicle and (b) the power required for the EM for the given speed profile

### 2.2 Battery model

A battery model is formed to find the state of charge (SOC) and battery voltage ($U_{Bat}$) according to the current demand ($I_{Bat}$) from the EM. SOC is calculated considering the battery voltage drops, which depend on the internal resistances (for charge and discharge) of the battery. The Simulink model of the battery is illustrated in Fig. 3a. The input and output parameters are shown in Fig. 3b for the battery subsystem. The battery model was constructed using an internal resistance model in which the open circuit voltage and the internal resistance ($R_{int}$) of the battery (while charging and discharging) are functions of SOC during the simulation time (Fig. 3c). These variables are taken from the Matlab/Simulink-based software called ADVISOR (Advanced Vehicle Simulator) for the Li-Ion battery module [25, 26]. Battery power is also calculated using the battery model to find fuel cell power requirements.

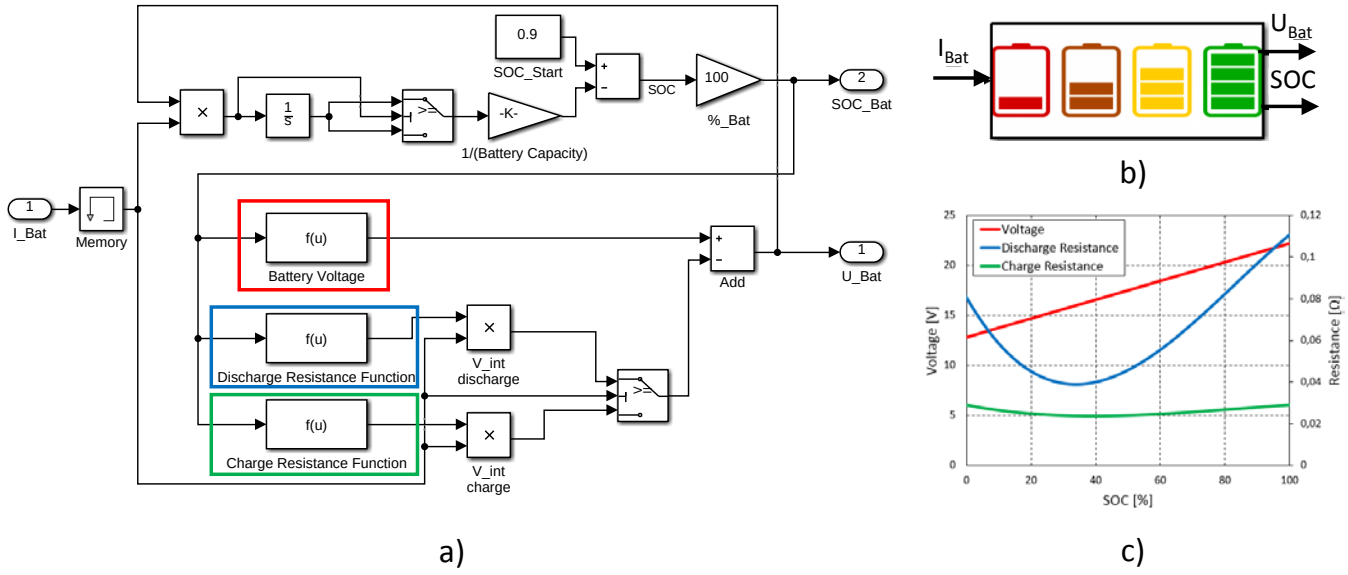


**Fig. 3** (a) Simulink model of the battery with its (b) input and output parameters and (c) the battery dynamics

The SOC for a given time and the required battery current ($I_{Bat}$) are found using Eqs. (8) and (9), respectively [5].

$$SOC(t) = SOC(0) - \frac{1}{C_{Bat}} \cdot \int_0^t I_{Bat} \cdot dt \tag{8}$$

$$I_{Bat} = \frac{V_{OCV} \pm \left( \sqrt{V_{OCV}^2 - 4 \cdot R_{\text{int}} \cdot P_{Bat}} \right)}{2 \cdot R_{\text{int}}} \tag{9}$$

where, $C_{Bat}$ is the total capacity [Wh] of the battery, $I_{Bat}$ is the battery current, $R_{int}$ is the internal resistance of battery, and $P_{Bat}$ is the power output of the battery.

### 2.3 DMFC system model

#### 2.3.1 Modeling approach and equations

The DMFC system consists of a DMFC stack, which is composed of 20 cells with 25 $cm^2$ active area each, a condenser, an anode mixing vessel, a circulating pump, a condensate pump, a methanol pump, an air blower, and a methanol tank as shown in Fig. 4. In this system, air reaches the cathode side after passing through an air blower and an air filter, respectively. At the cathode side, water is generated by the oxygen reduction reaction and the reaction of crossed-over methanol with oxygen. Some amount of water also exists at the cathode side because of the water crossover from the anode to the cathode. In addition, $CO_2$ is produced as a result of methanol reaction with oxygen. The fluid mixture consisting of $H_2O$, $CO_2$, $N_2$, and $O_2$ leaving the stack is cooled down and water is separated to liquid and gas phases after passing through a condenser. Then, liquid water is recycled to the anode mixing vessel and methanol reaches the anode mixing vessel from the methanol tank. This diluted methanol solution is pumped to the anode side. Unreacted methanol, $CO_2$ and water formed in the stack return to the anode mixing vessel; and $CO_2$, water vapour, and methanol vapour are released to the atmosphere from the top of the vessel.

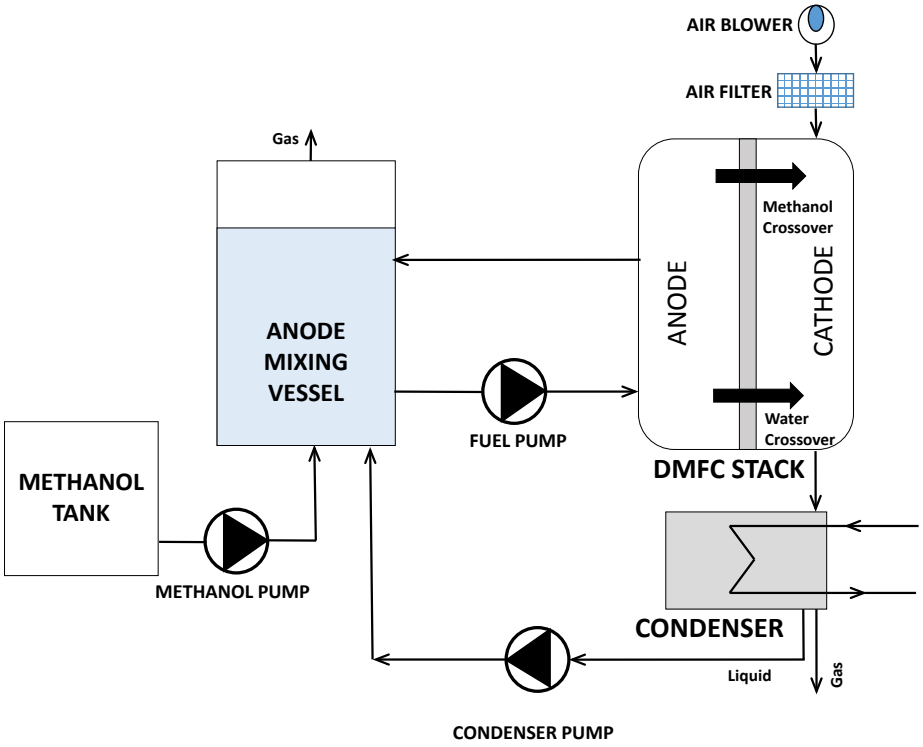


**Fig. 4** Layout of the DMFC system

In the DMFC sytem, five different fluids exist: methanol, water, oxygen, carbon dioxide, and nitrogen. Calculating the mass flow rate of these fluids at each point of the system is required in the system analysis. According to the Faraday's law, the overall methanol consumption rate [kg/h] in the stack can be expressed as:

$$\dot{m}_{CH_3OH,s} = \frac{(i_{el}+i_{perm})\cdot A_{cell}}{6\cdot F} \cdot n \cdot MW_{CH_3OH} \cdot 3.6 \quad (10)$$

where $i_{el}$ and $i_{perm}$ are the current density of the cell and the corresponding crossover current density, respectively. In this study, the value of $i_{perm}$ was obtained experimentally as discussed in Section 2.3.2. $A_{cell}$ is the superficial electrode area of the cell, $n$ is the number of cells, $MW$ represents the moleculer weight of the species, and $F$ is the Faraday's constant, which represents the charge per mole of equivalent electrons. The term stoichiometry ($\lambda$) is defined as a measure of the percent utilization of a reactant in a galvanic process. Its value is calculated according to the values of the cathode flow rate (CFR) and the anode flow rate (AFR), which are input parameters as shown in Section 2.3.2.

The net water production in the cathode is made up of four different sources: i) oxygen reduction reaction (ORR) that produces two moles of water per mole of methanol utilized at anode, ii) reaction of crossed-over methanol with oxygen at the cathode that produces two moles of water per mole of methanol utilized at anode, iii) the water crossed over from the anode, which is found experimentally for different operating conditions, and iv)

water vapor found in the air at the cathode inlet. Total water generation rate at the cathode [kg/h] by ORR:

$$\dot{m}_{w,el} = \frac{i_{el} \cdot A_{cell}}{2 \cdot F} \cdot n \cdot MW_{H_2O} \cdot 3.6 \quad (11)$$

Methanol permeation, which is defined as the methanol transport from anode to cathode, is a major problem as it decreases the cell voltage. When methanol reaches the cathode, the methanol reacts with oxygen and water is generated ($\dot{m}_{w,mc}$) [kg/h] as expressed in Eq. (12).

$$\dot{m}_{w,mc} = \frac{i_{perm} \cdot A_{cell}}{3 \cdot F} \cdot n \cdot MW_{H_2O} \cdot 3.6 \quad (12)$$

In this study, air entering the cathode is considered to be moist. The flow rate of water found in the moist air [kg/h] can be found by Eq. (13). In this equation, $y_i$ is the mole fraction of gas in air, $P_{sat}$ [bar] which is a function of temperature, is the saturation pressure of water at a given temperature and it can be calculated using Eq. (14) which is obtained using Engineering Equation Solver (EES) software [27] Here, $A$ is $2 \cdot 10^{-6}$, $B$ is $-9 \cdot 10^{-5}$, $C$ is 0.0029 and $D$ is 0.0063 for the the range of temperature of 1-100 °C. $\varphi$ is the relative humidity ratio which is defined as the ratio of partial pressure of water vapor to the saturation pressure.

$$\dot{m}_{w,a} = \frac{(i_{el}+i_{perm}) \cdot A_{cell}}{4 \cdot F} \cdot n \cdot \frac{\lambda c}{y_{O_2}} \cdot \sum(y_i \cdot MW) \cdot 3.6 \times 0.622 \times \frac{P_{sat} \cdot \varphi_{in}}{P - P_{sat} \cdot \varphi_{in}} \quad (13)$$

$$P_{sat} = A \cdot T^3 - B \cdot T^2 + C \cdot T - D \quad (14)$$

The $CO_2$ production rate at the cathode due to the methanol oxidation reaction (MOR) [kg/h] is

$$\dot{m}_{CO_2,c} = \frac{i_{perm} \cdot A_{cell}}{6 \cdot F} \cdot n \cdot MW_{CO_2} \cdot 3.6 \quad (15)$$

The $CO_2$ production rate at the anode due to the MOR [kg/h] is

$$\dot{m}_{CO_2,a} = \frac{i_{el} \cdot A_{cell}}{6 \cdot F} \cdot n \cdot MW_{CO_2} \cdot 3.6 \quad (16)$$

As illustrated in Fig. 4, there are mainly five auxiliary components (three pumps, a blower, and a water-cooled condenser) in the active DMFC system. In the hybrid model, a battery is considered to supply power for the blower and pumps. To find the power consumption in the blower and pumps, it is assumed that the pressure drops in the DMFC is approximately 200 Pa [28] and in the condenser is approximately 2 kPa [29].

The power consumptions in the blower and pumps [W] can be found using the following equation with the assumption that the fluids are incompressible:

$$\dot{W}_k = \frac{\dot{n}_j \cdot \Delta P \cdot v_j}{\eta_k} \quad (17)$$

Here, $k$ and $j$ subscripts represent the kind of an auxiliary equipments and species of fluid, respectively. $\Delta P$ is the pressure differences between inlet and outlet of the $k$ auxiliary equipment. $\dot{n}_j$ and $v_j$ are the molar flow rates and specific volume of $j$ species. $\eta_k$ represents the isentropic efficiency of the $k^{th}$ auxiliary equipment.

As discussed in this subsection, the DMFC system model is used to calculate the methanol consumption rate, the water and $CO_2$ production rates, and the power consumption in the blower and pumps. Methanol crossover rate, water crossover rate, and cell voltage of the single cell, which are measured experimentally (as discussed in Section 2.3.2), for different methanol concentrations and various current densities, are then integrated into Simulink model by surface block that creates a polynomial surface from the data (as discussed in Section 3). It should be also noted that all the cell performances are assumed to be the same; and thus, the cell model is implemented to stack model by simply multiplying the relevant variables (e.g. cell voltage and mass flow rates) with the number of cells.

**2.3.2 Experimental data used in the DMFC model**

Experimental data for DMFC operation were obtained in a custom-built single cell test rig. A membrane electrode assembley from Johnson Matthey Fuel Cells was used in a 17.64 cm² test cell with checkerboard anode and cathode flow fields machined into graphite plates. The dimensions of the channels such as the width of channels and lands was 1 mm each. PTFE flat gaskets were used for sealing. The cell was operated at 70 °C and methanol solution was pre-heated to that temperature before being fed into the cell. Permeation of water and methanol were determined by analyzing the air from the cathode exhaust. It was first heated to 130 °C to make

sure that all water is in the vapor phase. Here, water was detected by a humidity sensor. The air was then led through a condenser to remove water; and $CO_2$ concentration was measured by a $CO_2$ sensor. In previous experiments it was proven that all methanol permeating to the cathode is oxidized to $CO_2$ before leaving the cell. From the water and $CO_2$ concentrations and the air flow rates, the amounts of water and methanol permeated to the cathode were calculated. All the operating conditions were maintained for at least 30 minutes to assure that the cell is in equilibrium and averages of the last 15 minutes were taken as the results. Under some measurement conditions longer averaging times had to be used in order to obtain constant values for water permeation.

The voltage, methanol cross-over rates and water cross-over rates were obtained under different methanol concentrations, cathode volumetric flow rates, and current densities according to the procedure described in the paragraph above. The volumetric flow rate of dry air entering cathode ($\dot{V}_C$) was set to 15, 12 and 10 ml/(cm$^2$·min). The anode volumetric flow rate is taken as constant with a value of 0.2 ml/(cm$^2$·min). The setup is subjected to current densities in a range of 0.05-0.25 A/cm$^2$. 0.5 M, 0.75 M and 1 M methanol solution was fed to the cell from three different tanks. The results of these experiments are given in Fig. 5.

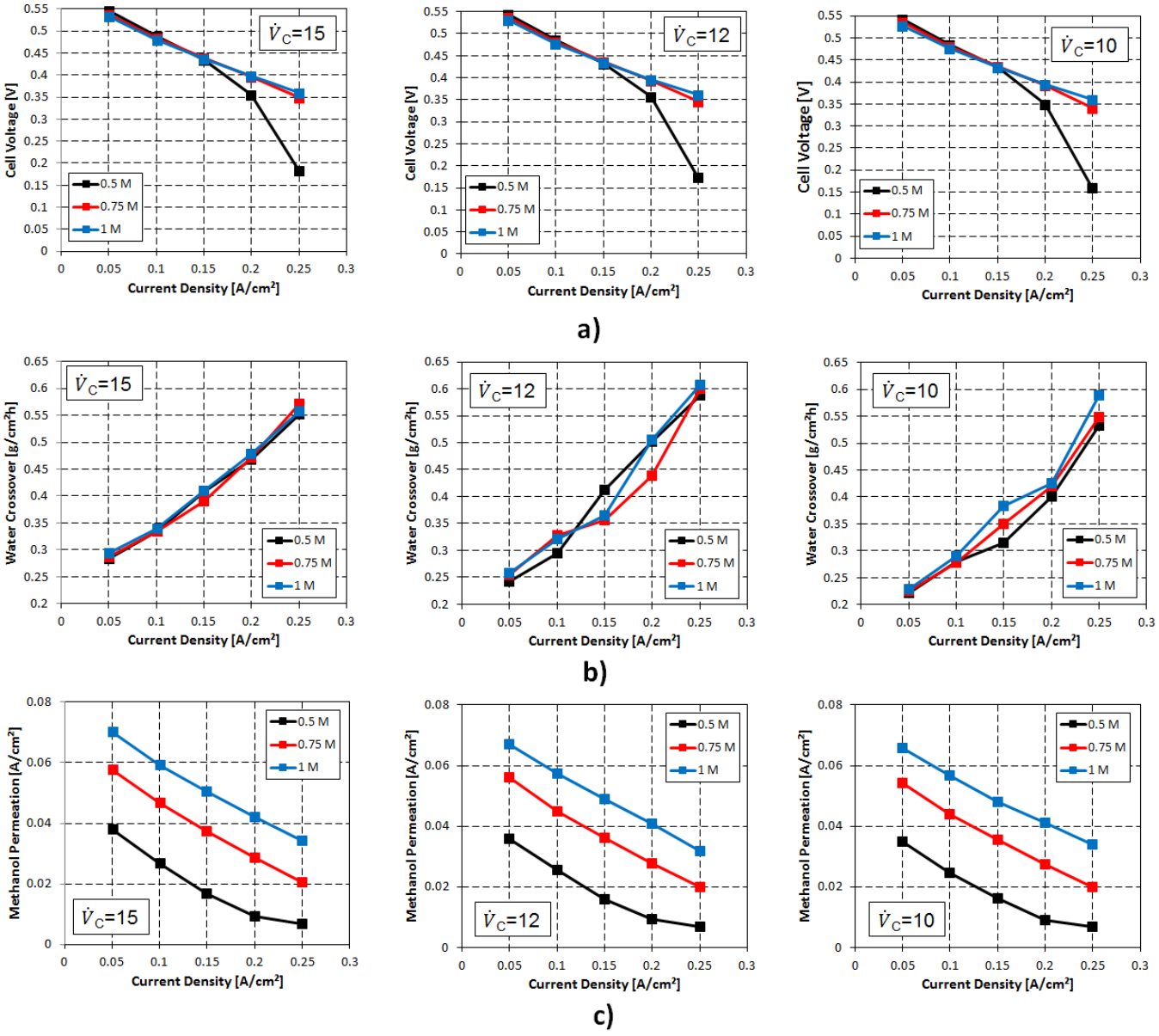


**Fig. 5** The effects of volumetric flow rate and methanol concentration on a) polarization curve, b) water crossover rate, and c) methanol permeation rate

The results seem to be compatible with the data given in literature [30-33]. It was found that when the current density is in the range of 0.2 A/cm$^2$ and 0.25 A/cm$^2$ at 0.5 M methanol solution, the cell voltage drops significantly. Apparently, this concentration is too low to obtain such high current densities. As also known, permeation of water and methanol is caused by two different mechanisms. The electroosmotic drag occurs due to the fact that the protons migrate through the membrane with the certain number of solvent moles [34]. Diffusion on the other hand is due to concentration differences between anode and cathode [35]. For water permeation, both mechanisms are

relevant, thus an increased water permeation is observed both for an increased current density and for an increased air flow rate, while the effect of methanol concentration on water permeation is negligible. Methanol permeation, however, depends mainly on methanol concentration and current density. A low methanol concentration means that the solvent moles permeating by electroosmotic drag are mainly water moles and the concentration gradient as driving force for methanol diffusion is low. High current densities mean that a lot of methanol is consumed for current generation. Together with a limited diffusion of methanol from the flow channels to the membrane surface, this results in a further reduction of methanol concentration at the membrane surface.

### 3. Simulation of the Hybrid Powertrain System

Hybrid powertrain model is formed in Matlab/Simulink environment according to the power requirement on the tire-road surface, which is an input parameter. The structure of the powertrain system used in the simulation of hybrid vehicle is shown in Fig. 6. The main system components and the connections among them are represented by the following parameters: voltage (*U*), current (*I*), current density (*i*), power (*P*), SOC, and state of fullness (*SOF*) of methanol for battery (*B*) and fuel cell (*FC*) with the subscripts i (*in*), o (*out*), B (battery), and FC (fuel cell).

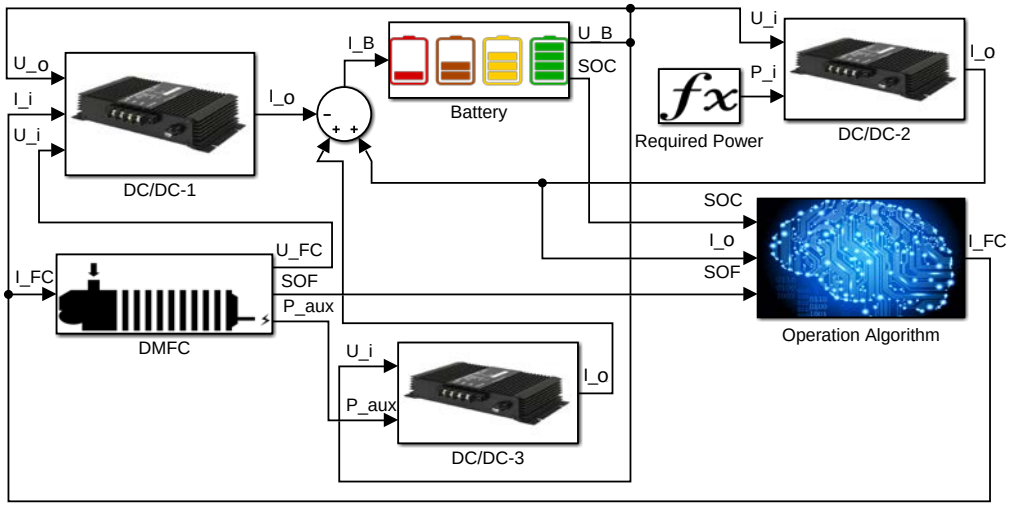


**Fig. 6** Simulation structure of the fuel cell hybrid vehicle system

A quasistatic method is applied for the analysis of the hybrid structure; and input and output parameters of the powertrain components are arranged according to this approach to perform the simulation. This method is similar to the method applied by Guzzella et al. [36] in which the power outputs and performances of each complex powertrain structures were investigated. This method offers design flexibility control for each subsystem to optimize the power flows in the powertrain system. Each powertrain element is illustrated with its input and output parameters using the basic blocks as shown in Fig. 7.

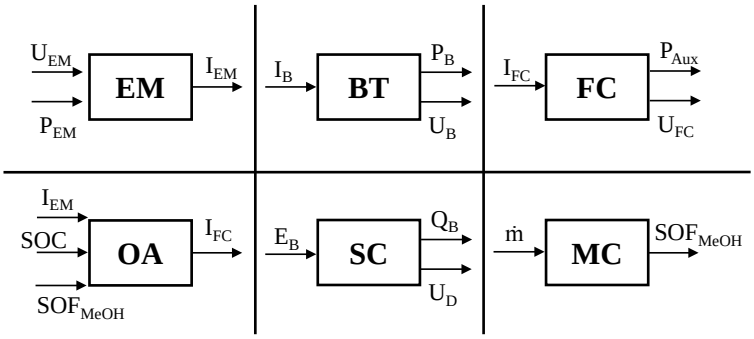


**Fig. 7** Parameters of the main blocks used in the quasistatic method for the system simulation (EM=Electric Motor, BT=Battery, FC=Fuel Cell, OS=Operation Strategy, SC=State of Charge, MC=Methanol Fuel Control).

Electric motor block (EM) calculates the current requirement ($I_{EM}$) of the electric motor by using the operating voltage ($U_{EM}$) and power ($P_{EM}$). If the SOC of battery is higher than 85%, operation algorithm block (OA) does not allow fuel cell (FC) operation and power input to auxiliary units, and current ($I_{FC}$) and voltage ($U_{FC}$) of FC have zero values. Battery is the only current source to respond the demand of EM when the FC is in the off mode. When the SOC is between 0% and 85%, the FC operates between the current density of 0.05 A/cm$^2$ and 0.25 A/cm$^2$. State of charge control block (SC), which is integrated into battery block (BT), uses energy consumption ($E_B$) as input and calculates the remaining battery capacity ($Q_B$) to determine the SOC and the voltage drops ($U_D$) as output parameters. Methanol fuel control (MC) works inside the FC block to calculate the state of fullness of methanol in

storage tank ($SOF_{MeOH}$) as output parameter depending on the methanol consumption rate ($\dot{m}_{CH3OH,s}$ as shown in Eq. (10)); and the information about methanol state in the tank is transmitted to the OA block to control the FC operation.

Detailed operational algorithm is illustrated in Fig. 8 for each simulation time step. Operational algorithm uses power demand from EM and vehicle speed profile as input parameters for each time step of the simulation. After the calculation of the required current according to the constant operation voltage of EM, the algorithm controls the current and if it is equal with zero, it means the vehicle is stopping and the DMFC stack is not allowed to produce any current. The DMFC stack maintains the off mode until the SOC reaches to 85% of the battery capacity. Required current density of the DMFC increases from 0.05 A/cm$^2$ to 0.25 A/cm$^2$ linearly between 85% and zero capacity of the battery. According to the single cell experimental results, current density range is divided into three sections to apply more realistic operation parameters for better performance results of DMFC stack. Test results show better voltage output from single cell, between 0.05 A/cm$^2$ to 0.15 A/cm$^2$ for 0.5 M, between 0.15 A/cm$^2$ to 0.2 A/cm$^2$ for 0.75 M, and between 0.2 A/cm$^2$ to 0.25 A/cm$^2$ for 1 M methanol concentrations. In addition, lower cathode volumetric flow rate ($\dot{V}_C$) causes lower methanol permeation, lower water crossover, and lower blower power requirement for same methanol concentrations. Therefore, voltage output, methanol permeation, and water crossover results of a single DMFC are given at 10 ml/cm$^2$·min $\dot{V}_C$ and 0.5 M between 0.05 A/cm$^2$ to 0.15 A/cm$^2$, 12 ml/cm$^2$·min $\dot{V}_C$ and 0.75 M between 0.15 A/cm$^2$ to 0.2 A/cm$^2$, and 15 ml/cm$^2$·min $\dot{V}_C$ and 1 M between 0.2 A/cm$^2$ to 0.25 A/cm$^2$ as long as methanol is fed from the storage tank to the DMFC stack. If there is no methanol left in the storage tank, battery only supplies EM. After the last time step or when the battery capacity reaches at 0% SOC, the simulation stops.

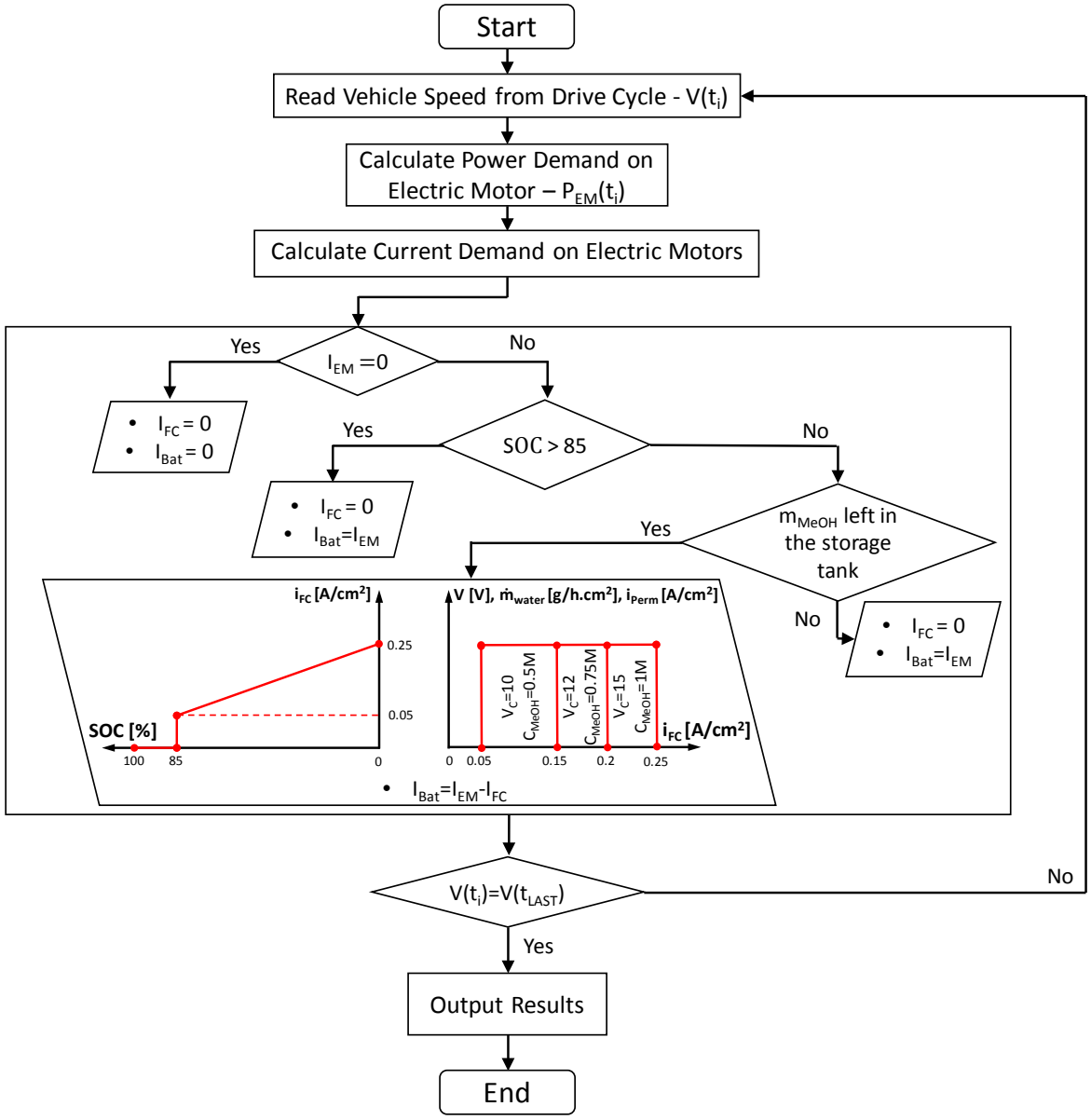


**Fig. 8** Flowchart of the operation algorithm for system simulation.

## 4. Results and discussion

Required power for the traction of a vehicle is produced by the electric motor for one drive cycle (70 seconds). Simulation of the DMFC based hybrid system, which uses this power requirement as the input parameter in this vehicle, was performed in Matlab/Simulink environment for 100 drive cycle time. The following simulation configuration parameters were used: maximum step size of $3x10^{-4}$, relative tolerance of $3x10^{-4}$, and solver type as Ordinary Differential Equation (ODE 45). The power outputs of EM and battery, the change of SOC, and the power consumption of auxiliary units of the DMFC system and the power output of DMFC stack with respect to the simulation time are presented in Figs. 9a-9c, respectively. Fig. 9a shows that decreases in the battery power output can be clearly observed from the time that DMFC starts to operate to the end of the simulation. Maximum power output difference between the EM and the battery, which is the same with the power output of the DMFC, occurs at the end of simulation since the highest power from the DMFC is required at the lowest SOC level. The results of the simulation also show that just before the 250$^{th}$ second after the start of the simulation, the SOC of the battery drops from its initial condition (90% level) to 85% level (Fig. 9b) and DMFC starts to operate with around 17 W power output (Fig. 9c). On the other hand, at the 6500$^{th}$ second of the simulation (end of the simulation), the SOC level drops to 0%, while the power output of the DMFC is 45 W. It can be seen from Fig. 9c that as the current demand increases, there is a small increase in the power consumption of the auxiliary components; however, there is a significant increase in the power output of the DMFC. Especially, the effects of changing cathode air inlet flow rate and methanol concentration can be observed clearly as sudden increments of 3-4 W at around the 3100$^{th}$ second and the 4800$^{th}$ second of the simulation.

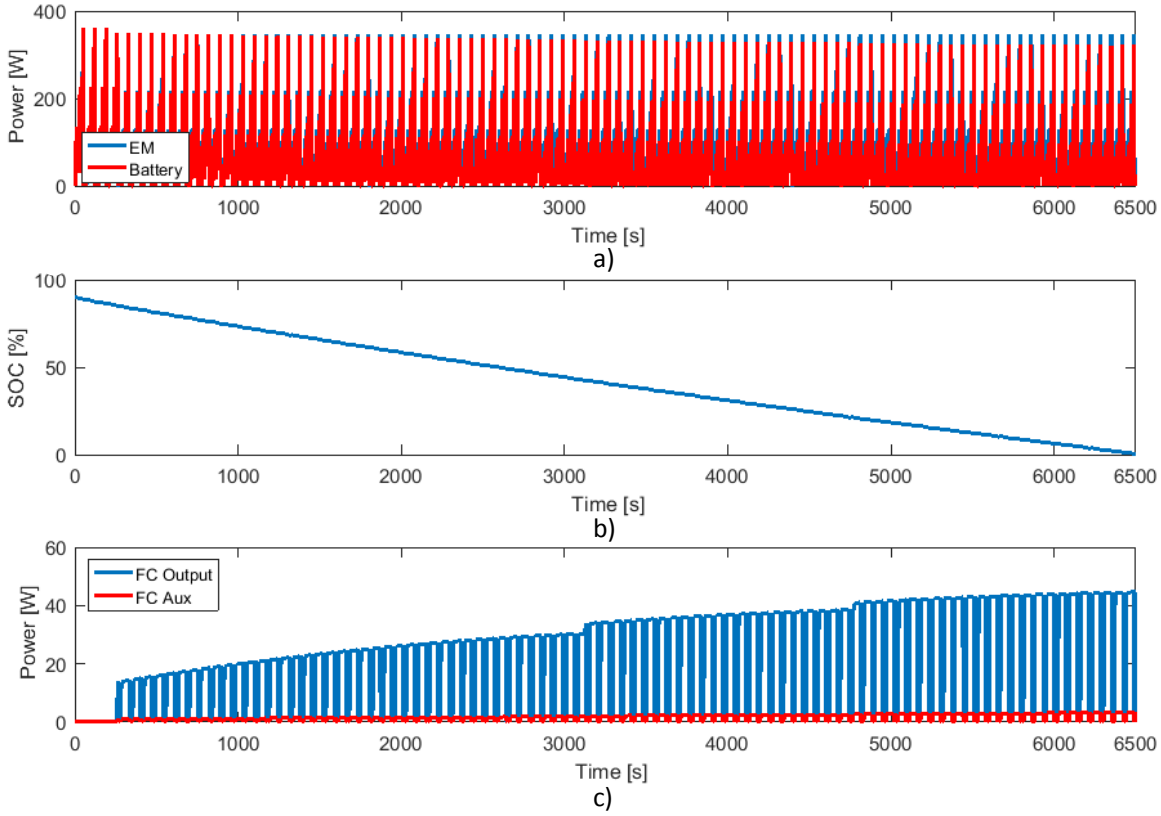


**Fig. 9** Simulation results for (a) power demand from EM and battery, (b) SOC history of battery, and (c) power output of the DMFC stack and power required for the auxiliary components of the DMFC system

The water production rate due to electrochemical reactions, methanol crossover, water crossover, and water vapour in the cathode inlet are presented in Figs 10a-10d, respectively. During the simulation time, the mass flow rate of water production by the electrochemical reaction increases linearly as shown in Fig 10a. This can be explained by the increasing current density according to the operation algorithm (as can be seen from Eq. (11)). It can be seen from Fig. 10b that the water production rate due to methanol crossover decreases with increasing current density up to the next step of operation as the methanol crossover also decreases with increasing current density. The system operates at higher methanol concentration and cathode volumetric flow rate in the next steps of the operation according to the required current density as shown Fig. 8. This operational change leads to higher water production flow rate due to methanol crossover. Fig. 10c shows that water production rate due to water crossover, which is mainly a function of operating temperature, membrane properties, methanol concentration, and current density [37,38], increases with increasing current density. Fig. 10d shows that water production rate due to water vapour found in the cathode inlet increases significantly only after the cathode flow rate changes. In total, water production at the cathode is dominated by water crossover and the electrochemical reaction, while methanol

crossover and water vapour in the cathode inlet are 1-2 orders of magnitude smaller.

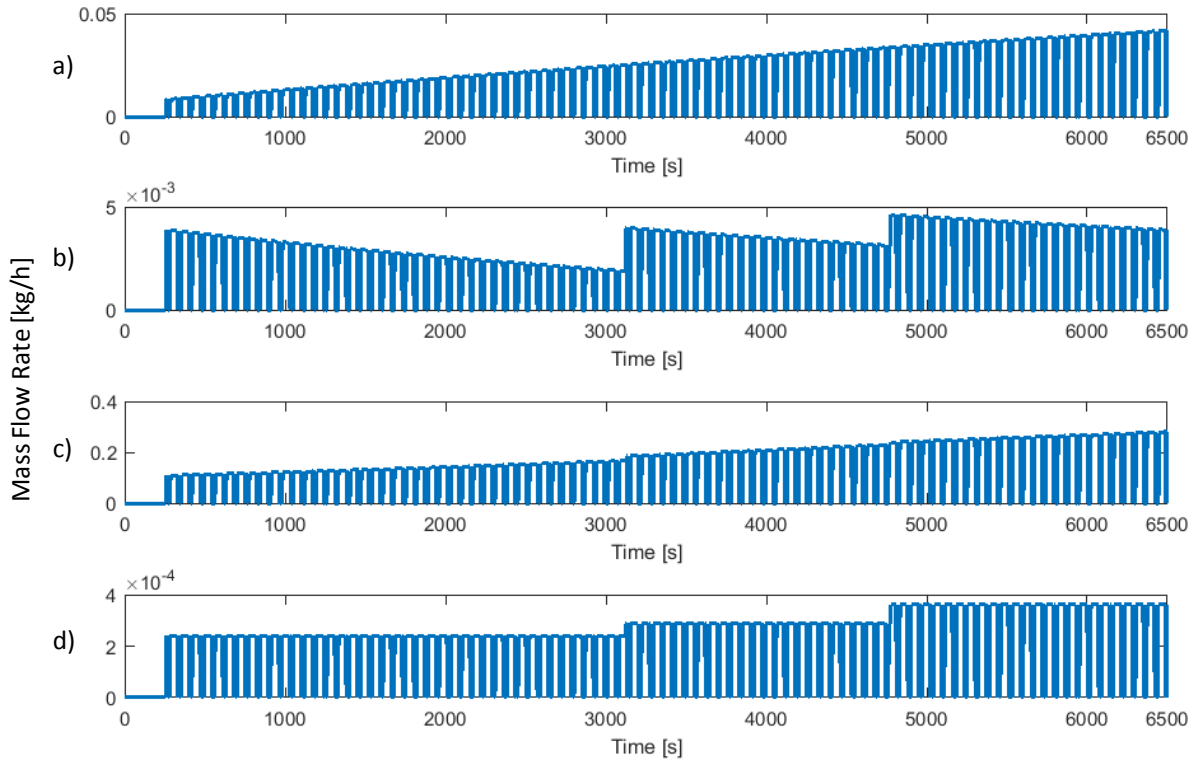


**Fig. 10** Simulation results for water production of DMFC stack by (a) electrochemical reactions (b) methanol crossover (c) water crossover, and (d) water vapour in the cathode inlet

As discussed in Section 2.3.1, $CO_2$ is produced at the anode and cathode sides due to MOR (Eq. (15) and (16)); while methanol is consumed due to MOR and methanol crossover (Eq. (10)). The total amount of $CO_2$ production and methanol consumption through the simulation time are presented in Fig. 11. It can be observed that $CO_2$ production and methanol consumption, which mainly depend on current density and methanol crossover density, increase to approximately 32 g and 23 g, respectively, at the end of the simulation.

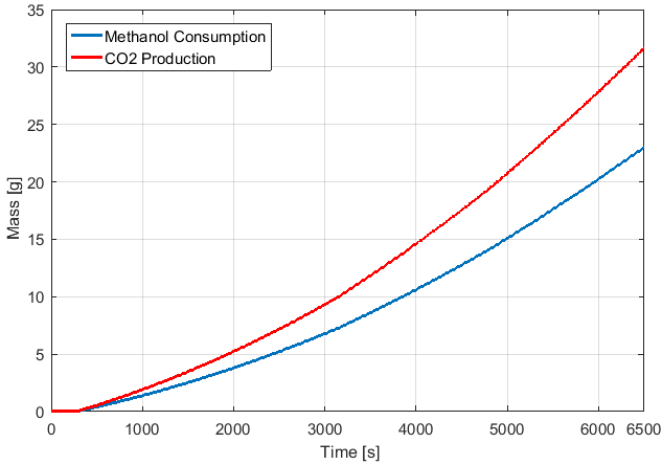


**Fig. 11** Simulation results of (a) methanol consumption and (b) $CO_2$ production in the DMFC stack

## 5. Conclusions

System simulation for a DMFC hybrid vehicle was performed using a quasistatic method in Matlab/Simulink environment. This method is based on a semi-theoretical approach in which experimental DMFC results are combined with modeling equations. The simulation gives power outputs of each component in the drivetrain and the amounts of methanol consumption, water production, and $CO_2$ emission of the system during its operation. Operation parameters such as cathode flow rate and methanol concentration are arranged according to the results obtained from the single cell experiments to simulate a realistic and reliable operation of DMFC. In this arrangement, the operating range of DMFC is divided into three sections for three different values of methanol concentration and cathode flow rate according to the current density demand.

The main conclusions of this study are listed below.

- The total power consumption of the auxiliary components is about 5 W for the maximum current demand at the lowest SOC (at the end of the simulation). At this condition, the power output of the DMFC is 45 W. Power output of DMFC increases by 5 W and 4 W, respectively, when higher values of cathode flow rate and methanol concentration are started to be used when the current density is taken as 0.15 A/cm$^2$ and 0.2 A/cm$^2$. However, at these conditions, methanol crossover and water crossover in the DMFC stack also increase.
- The production of water due to electrochemical reactions and water crossover reach 0.045 kg/h and 0.3 kg/h at the end of simulation. On the other hand, water production due to methanol crossover and water vapour inside the cathode inlet are relatively negligible.
- Total $CO_2$ production in the DMFC stack due to MOR at the anode and the reaction of methanol crossover with oxygen at the cathode is 32 g. Total methanol consumption is calculated as 23 g for the given simulation time.

This study presents a method for the simulation of a DMFC hybrid powertrain system used in a small sized vehicle through the implementation of experimental fuel cell data into the operational algorithm of the system. The innovative method given in this study can guide researchers, engineers, and scientists to develop more energy-efficient and environmentally-friendly DMFC based hybrid vehicles. In a future study, a more comprehensive semi-theoretical model can be developed considering stack-level experimental data and mass and energy balances for all components of the DMFC subsystem.

**Acknowledgements**

This work has been supported by Dokuz Eylul University Department of Scientific Research Projects with the project number 2017.KB.FEN.005.

**References**

[1] Zago M, Casalegno A, Santoro C, Marchesi R. Water transport and flooding in DMFC: Experimental and modeling analyses. Journal of Power Sources 2012; 217: 381-391.

[2] Colpan CO, Dincer I, Hamdullahpur F.. Portable fuel cells–Fundamentals, technologies and applications. In Mini-Micro Fuel Cells (pp. 87-101). Springer 2008, Dordrecht.

[3] Huang HP, Kuo JK, Han CY. Numerical investigation into slope-climbing capability of fuel cell hybrid scooter. Applied Thermal Engineering 2017;110:921-90.

[4] Samsun RC, Krupp C, Baltzer S, Gnörich, B, Peters R, Stolten D. A battery-fuel cell hybrid auxiliary power unit for trucks: Analysis of direct and indirect hybrid configurations. Energy Conversion and Management 2016;127:312-323.

[5] Li J, Wang Y, Chen J, Zhang X. Study on energy management strategy and dynamic modeling for auxiliary power units in range-extended electric vehicles. Applied Energy 2017;194:363-375.

[6] Marzougui H, Amari M, Kadri, Bacha F, Ghouili J. Energy management of fuel cell/ battery/ ultracapacitor in electrical hybrid vehicle. Int J of Hydrogen Energy 2017;42:8857-8869.

[7] Marx N, Hissel D, Gustin F, Boulon L, Agbossou K. On the sizing and energy management of an hybrid multistack fuel cell - Battery system for automotive applications. Int J of Hydrogen Energy 2017;42:1518-1526.

[8] Li T, Liu H, Zhao D, Wang L. Design and analysis of a fuel cell supercapacitor hybrid construction vehicle. Int J of Hydrogen Energy 2016;41:12307-12319.

[9] Li J, Hu Z, Xu L, Ouyang M, Fang C, Hu J, Cheng S, Po H, Zhang W, Jiang H. Fuel cell system degradation analysis of a Chinese plug-in hybrid fuel cell city bus. Int J of Hydrogen Energy 2016;41:15295-15310.

[10] Mokrani Z, Rekioua D, Mebarki N, Rekioua T, Bacha S. Proposed energy management strategy in electric vehicle for recovering power excess produced by fuel cells.Int J of Hydrogen Energy 2017;42:19556-19575.

[11] Hwang JJ, Chen YJ, Kuo JK. The study on the power management system in a fuel cell hybrid vehicle. Int J of Hydrogen Energy 2012;37:4476-4489.

[12] Zheng CH, Oh CE, Park YI, Cha SW. Fuel economy evaluation of fuel cell hybrid vehicles based on equivalent fuel consumption. Int J of Hydrogen Energy 2012;37:1790-1796.

[13] Atacan OF, Ouellette D, Colpan CO. Two-dimensional multiphase non-isothermal modeling of a flowing electrolyte–Direct methanol fuel cell. International Journal of Hydrogen Energy 2017; 42:2669-2679.

[14] Yang Q, Kianimanesh A, Freiheit T, Park SS, Xue D. A semi-empirical model considering the influence of operating parameters on performance for a direct methanol fuel cell. Journal of Power Sources 2011;196:10640-10651.

[15] Ge J, Liu H. A three-dimensional mathematical model for liquid-fed direct methanol fuel cells. Journal of Power Sources 2006;160:413-421.

[16] Kulikovsky AA. Optimal temperature for DMFC stack operation. Electrochimica Acta, 2008;53:6391-6396.

[17] McIntyre J, Kulikovsky AA, Müll M, Stolten D. Large‐scale DMFC Stack Model: Feed Disturbances and Their Impact on Stack Performance. Fuel Cells 2012;12:1032-1041.

[18] Kablou Y, Cruickshank CA, Ouellet D, Matida E. (2011, January). Semi-Empirical Flow and Pressure Distribution Modeling of a Flowing Electrolyte Direct Methanol Fuel Cell Stack. In ASME 2011 9th International Conference on Fuel Cell Science, Engineering and Technology collocated with ASME 2011 5th International Conference on Energy Sustainability (pp. 677-683). American Society of Mechanical Engineers.

[19] Andrian VS, Meusinger J. Process analysis of a liquid-feed direct methanol fuel cell system. J of Power Sources 2000;91:193-201.

[20] Dohle H, Mergel J, Stolten D. Heat and power management of a direct-methanol-fuel-cell (DMFC) system. J. of Power Sources 2002;111:268-282.

[21] Jiang R, Chu D. Water crossover: a challenge to DMFC system II. Simulation of water recycling in a 20 W DMFC system. J of the Electrochemical Society 2008;155:804-810.

[22] Na Y, Zenith F, Krewer U.. Highly integrated direct methanol fuel cell systems minimizing fuel loss with dynamic concentration control for portable applications. Journal of Process Control 2017;57:140-147.

[23] Zenith F, Na Y, Krewer U.. Effects of process integration in an active direct methanol fuel-cell system. Chemical Engineering and Processing Process Intensification 2012; 59: 43-51.

[24] Fernandez RA, Cilleruelo FB, Martinez IV. A new approach to battery powered electric vehicles: A hydrogen fuel-cell-based range extender system. Int J of Hydrogen Energy 2016;41:4808-4819.

[25] Turkmen AC, Solmaz S, Celik, C. Analysis of fuel cell vehicles with advisor software. Renewable and Sustainable Energy Reviews 2017;70: 1066-1071.

[26] Same A, Stipe A, Grossman D, Park JW. A study on optimization of hybrid drive train using Advanced Vehicle Simulator (ADVISOR). Journal of Power Sources 2010;195: 6954-6963.

[27] Klein S, Alvarado F. Engineering equation solver, F-chart software, Middleton, WI, 1996.

[28] Müller M, Kimiaie N, Glüsen A., Stolten D. (). The Long Way of Achieving a Durability of 20,000 h in a DMFC System. Advances in science and technology 2014; 93:56-60. Trans Tech Publications.

[29] Hwang YW, Kim MS. The pressure drop in microtubes and the correlation development. International Journal of Heat and Mass Transfer 2006; 49:1804-1812.

[30] Nakagawa N, Xiu Y. Performance of a direct methanol fuel cell operated at atmospheric pressure. Journal of Power Sources 2003;118:248-255.

[31] Wang Q, Wang G, Lu X, Chen C, Li, Z, Sun G. Investigation of Methanol Crossover and Water Flux in an Air-Breathing Direct Methanol Fuel Cell. Int. J. Electrochem. Sci. 2015;10:2939-2949.

[32] Ge J, Liu H. Experimental studies of a direct methanol fuel cell. Journal of Power Sources 2005;142:56-69.

[33] Falcão DS, Oliveira VB, Rangel CM, Pinto AMFR. Experimental and modeling studies of a micro direct methanol fuel cell. Renewable Energy 2015;74:464-470.

[34] Ren XM, Henderson W, Gottesfeld S. J of the Electrochemical Society 1997;144:L267-L270.

[35] Gogel V, Frey T, Yongsheng Z, Friedrich KA, Jörissen L, Garche, J. Performance and methanol permeation of direct methanol fuel cells: dependence on operating conditions and on electrode structure. J of Power Sources 2004;127:172-180.

[36] Guzzella L, Sciarretta A. Vehicle Propulsion Systems Introduction to Modeling and Optimization. Springer 2005.

[37] Lu GQ, Liu FQ, Wang CY. Water transport through Nafion 112 membrane in DMFCs. Electrochemical and Solid-State Letters 2005;8:A1-A4.

[38] Kim L D, Park CH, Tocci E, Nam SY. Experimental and modeling study of blended membranes for direct methanol fuel cells. Journal of Membrane Science 2018;564:308-316.

[39] Wei L, Yuan X, Jiang F. A three-dimensional non-isothermal model for a membraneless direct methanol redox fuel cell. J of Power Sources 2018;385:130-140.

[40] Chen X, Li T, Shen J, Hu Z. From structures, packaging to application: a system-level review for micro direct methanol fuel cell. Renewable and Sustainable Energy Reviews 2017;80:669-678.

[41] Chen X, Shen J, Hu Z, Huo X. Manufacturing methods and applications of membranes in microfluidics. Biomedical Microdevices 2016;18(6):1-13.

[42] Xia Z, Sun R, Jing F, Wang S, Sun H, Sun G. Modeling and optimization of Scaffold-like macroporous electrodes for highly efficient direct methanol fuel cells. Applied Energy 2018;221:239-248.